Ethanol Conversion to Butanol over Small Coinage Metal Clusters: An Experimental and Computational Study

Article *in* Journal of Cluster Science · August 2022

DOI: 10.1007/s10876-022-02344-0

CITATIONS
0

READS
84

6 authors, including:

Godfrey Barasa
Jaramogi Oginga Odinga University of Science and Technology
24 PUBLICATIONS **118** CITATIONS
SEE PROFILE

Gershom Mutua
Masinde Muliro University of Science and Technology
14 PUBLICATIONS **50** CITATIONS
SEE PROFILE

Hitler Louis
University of Calabar
215 PUBLICATIONS **1,977** CITATIONS
SEE PROFILE

Wu Haiming
Chinese Academy of Sciences, Institute of Chemistry
44 PUBLICATIONS **289** CITATIONS
SEE PROFILE

Journal of Cluster Science
https://doi.org/10.1007/s10876-022-02344-0

ORIGINAL PAPER

Ethanol Conversion to Butanol over Small Coinage Metal Clusters: An Experimental and Computational Study

Anthony M. S. Pembere[1] · Denis Magero[2] · Godfrey O. Barasa[1] · Gershom Kyalo Mutua[3] · Hitler Louis[5] · Haiming Wu[4]

Received: 17 June 2022 / Accepted: 5 August 2022

Abstract

We illustrate the mechanism for the C–O, C–H and O–H bond activation in the coupling of ethanol to butanol over small coinage clusters (copper, silver and gold). It is found that charge transfer interactions between the clusters and the alcohol initiate their reactions allowing a chemisorption step. The binding energy is calculated, whereby ethanol adsorbs very strongly on Au in comparison to Ag and Cu. The nature of bonding is investigated using natural bond orbital (NBO) analysis and quantum theory of atoms-in-molecules (QTAIM). The reactive intermediates, activated complexes, transition states, and bond breaking on icosahedral $Au_{13,}$ Cu_{13}, Ag_{13} and also triangular $Au_{3,}$ Cu_3, Ag_3 have been calculated alongside the cycle kinetics. Furthermore, high resolution mass spectroscopy has been used to study the ethanol coupling reactions over small Au cluster catalysts. The observation of the coupling products concurs with the kinetic- and thermodynamic- allowed reaction pathway of Guerbet coupling of ethanol. The highest selectivity for butanol (61%) is obtained after a reaction time of 2 h while the highest ethanol conversion (91%) is obtained after a reaction time of 5 h.

Keywords Coinage Metal Cluster · Density functional theory · Guerbet Reaction · Catalytic conversion · Ethanol · Butanol

Introduction

Development of sustainable energy sources is a key goal of the research community [1]. The use of fossil fuels has various complex issues which are well-documented [2]. The merits of moving to a sustainable energy portfolio are clear [3]. Compared to gasoline, ethanol has many notable drawbacks such low energy density, high water absorption and dilution problems in tanks [3]. However, there is a high similarity in properties between butanol and gasoline which can be exploited. [3]. Among the interesting fuel properties of n-butanol include non-corrosivity, immiscibility with water, and high energy density (90% that of gasoline) [4]. However, butanol from biological raw materials remains a challenge [5]. A catalytically assisted conversion of ethanol to butanol (Guerbet reaction) is being considered as a viable alternative [6]. The Guerbet synthesis is named after the scientist Marcel Guerbet who studied the self-coupling of alcohols [2]. This reaction allows a primary or secondary alcohol to be condensed with itself or with another alcohol, thus to convert simple inexpensive feedstocks into more valuable products. While this appears to be a simple reaction, there are various challenges especially on the selectivity since the n-butanol formed can couple with higher alcohols [6]. A variety of catalysts has been applied in the conversion of ethanol to butanol. [7] For example, catalyst doped with Cu and Ni have recorded good catalytic activities with ethanol conversion and n-butanol yield of 56% and 22%, respectively [8]. Elsewhere, coupling reactions of methanol, ethanol and *n*-butanol at temperatures below 100 °C by unsupported

✉ Anthony M. S. Pembere
apembere@jooust.ac.ke

✉ Haiming Wu
hmwu88@iccas.ac.cn

1 Department of Physical Sciences, Jaramogi Oginga Odinga University of Science and Technology, P.O Box 210, Bondo 40601, Kenya

2 Department of Chemistry and Biochemistry, Alupe University College, P.O Box 845, Busia 50400, Kenya

3 Department of Pure and Applied Chemistry, Masinde Muliro University of Science and Technology, P.O Box 190, Kakamega 50100, Kenya

4 Department of Pure and Applied Chemistry, University of Calabar, Calabar, Nigeria

5 State Key Laboratory for Structural Chemistry of Unstable and Stable Species, Institute of Chemistry, Chinese Academy of Sciences, Beijing, China

Published online: 26 August 2022

nano-porous Au catalysts has been studied, opening the door to a molecular-level understanding of the reaction [9].

It is worth noting that the over the last few years, research interests in cluster science of coinage metals is fast expanding [10]. There are reports of successful synthesis of metallic nanoclusters (NC) with monocrystalline structure containing metal-to-metal bonds. On the other side [11], metal clusters in gaseous phase are best for studying properties of the metals. Generally, when the size of the metal cluster is small ($n < 10$), addition of extra atoms or electrons may result in unpredictable changes in its property with considerable dependence on size· [12]. This is clear indication that each atom plays an important role in the cluster [10]. Based on this, we have investigated the conversion of ethanol on typical coinage clusters. Using DFT calculations, we have firstly examined the structure chemistry, bonding and reaction paths of the thirteen atom clusters (Ag_{13}, Au_{13} and Cu_{13}) and also the three atom clusters (Ag_3, Au_3 and Cu_3). Interestingly, Furthermore, we have studied the ethanol coupling reactions using high resolution mass spectroscopy over the small Au cluster catalysts, prepared by laser ablation method followed by careful separation techniques. The observed coupling products agrees with the kinetic- and thermodynamic- allowed reaction pathways of Guerbet coupling of ethanol.

Computational and Experimental Methods

We used the GGA with the PBE exchange–correlation functional that has been found to be suitable in describing the exchange and correlation effects [13–17]. Geometry optimizations and energy calculations were done using $DMol^3$ code [18, 19]. The double numerical plus p-functions (DNP) basis set was used [20]. The transition states were located using the synchronous method with conjugated gradient refinements. This involve linear synchronous transit maximization, followed by repeated conjugated gradient minimizations, and then quadratic synchronous transit maximizations and repeated minimizations until a transition state is located [21]. NBO analysis was done using Gaussian 09 [22], at B3LYP level of theory. The LanL2DZ and 6–31 + G(d) for the heavy (Cu, Ag, and Au) and representatively elements (H, C, O) respectively was specified. Multiwfn 3.7 dev was used for the quantum theory of atoms-in-molecules (QTAIM) investigations and all other wavefunction analyses [23]. The respective cycle kinetics were modeled using the energetic span model [24, 25].

The experimental results were obtained using a modified container for laser ablation in liquid as reported in our previous reports [26, 27]. Pure gold clusters were obtained by laser ablation of gold in water [26, 27]. The ablation process was carried out in ultra-pure water and product solution filtered off. The obtained solution was concentrated to 5 ml. Afterwards, about 1 ml of absolute ethanol was added and the reaction allowed to proceed for 1,2,3,4 and 5 h at 70 ℃ prior to mass spectrometric analysis. Blank experiments were also carried out following the above described procedure but without adding the as-prepared gold clusters.

Results and Discussion

The 13-atom metal clusters have special electronic configuration [12, 13]. and therefore they are ideal systems for computational modelling as they possess exceptional stability and less site-selectivity especially in icosahedral or tetra-decahedral structured systems [28] For example, they have been used as models in the CO oxidation [14]. It has also been reported that in aqueous media Au_{13} clusters have good stability relative to other cluster sizes. Therefore, they can provide atomistic details of growth by cluster coalescence [29]. Figure 1 shows a plot of the frontier orbitals and corresponding geometry of Ag_{13}, Au_{13} and Cu_{13} clusters. The HOMO does indicate the Lewis acid sites while the LUMO, Lewis base sites [30–34]. It is seen that HOMO in Au_{13} cluster is generally at edge sites while LUMO is at the center of the cluster. For the case of $Cu_{13,}$ the HOMO is at the center while LUMO is at the edge sites. The frontier orbitals for $Ag_{13,}$ are located on different atoms at the edge. Table 1 presents a comparison of the HOMO and LUMO energies. Ag_{13} has relatively higher HOMO and LUMO energies compared to Au_{13} and Cu_{13}. Also, Ag_{13} has also a higher HOMO–LUMO gap. From energy differences between the HOMOs of $Au_{13}/Ag_{13}/Cu_{13}$ and the LUMO of ethanol, it is expected that charge transfer occurs rendering reaction with CH_3CH_2OH. The global electrophilicity indices, of Au_{13}, Ag_{13}, Cu_{13} and CH_3CH_2OH have also been examined [35–37]. The global reactivity descriptors (chemical potential μ, electronegativity χ, chemical hardness η, electrophilicity ω, and chemical softness S) can be calculated using [38];

$$-\mu = 1/2\left(E_{HOMO} + E_{LUMO}\right) = \chi \tag{1}$$

$$\eta = 1/2(IP - EA) = \frac{E_{LUMO} - E_{HOMO}}{2} \tag{2}$$

$$\omega = \frac{\mu^2}{2\eta} \tag{3}$$

$$S = \frac{1}{2\eta} = \frac{1}{IP - EA} = \frac{1}{E_{LUMO} - E_{HOMO}} \tag{4}$$

The global reactivity parameters of the studied compounds are presented in Table 1. The calculated electronegativity and chemical hardness of ethanol is found to be

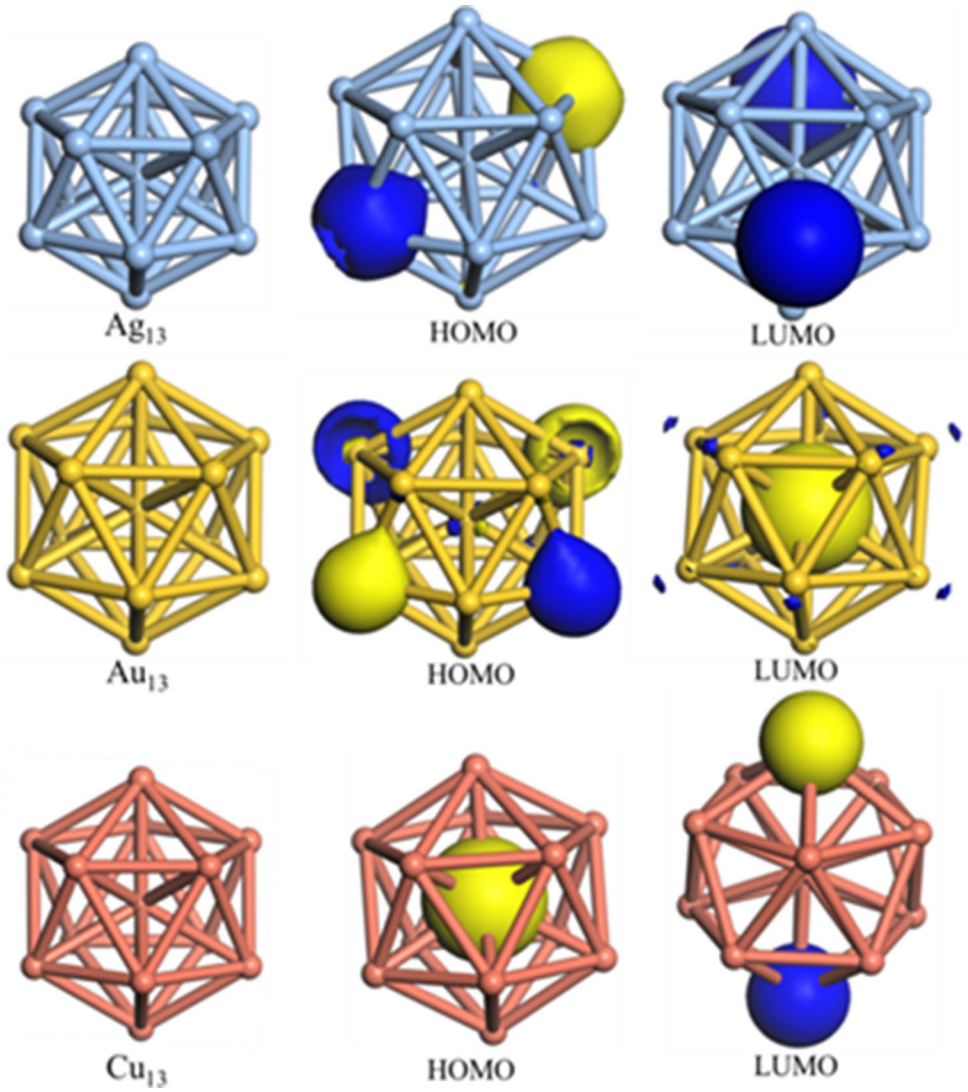

Fig. 1 Optimized structures and frontier orbitals of Ag_{13}, Au_{13} and Cu_{13}

Table 1 Energies of the frontier molecular orbitals and the global electrophilicity indices

	E_{HOMO} (eV)	E_{LUMO} (eV)	HOMO–LUMO gap (eV)	η (eV)	μ (eV)	χ (eV)	ω (eV)
Ag_{13}	− 5.71	− 4.08	1.63	0.815	− 4.90	4.90	14.70
Au_{13}	− 3.81	− 3.27	0.54	0.270	− 3.54	3.54	23.21
Cu_{13}	− 4.76	− 4.69	0.07	0.035	− 4.72	4.72	318.94
CH_3CH_2OH	− 7.08	− 4.62	2.46	1.23	− 5.85	5.85	13.91

higher than that of $Au_{13,}$ Ag_{13} and Cu_{13} clusters (Table 1). Therefore, along a polar interaction, the net charge transfer exists, from ethanol to the clusters.

We have investigated the adsorption of CH_3CH_2OH on Ag_{13}, Au_{13}, Cu_{13} (Fig. 2). Among the binding energies, Au_{13} exhibits relatively higher value. Natural bond orbital (NBO) analysis was also carried out to get insights into the interactions between the Lewis type and non-Lewis type orbitals of the cluster-ethanol adducts. The interaction was expressed in terms of charge exchange and conjugative interaction between acceptor and donor orbitals together with charge delocalization (natural charge) [39, 40]. The NBO analysis was performed by considering the changes in the highest energy of interaction between donors and acceptor NBOs. As seen in Table 2, the highest stabilization energies for the Ag_{13}-ethanol, Au_{13}-ethanol, and Cu_{13}-ethanol

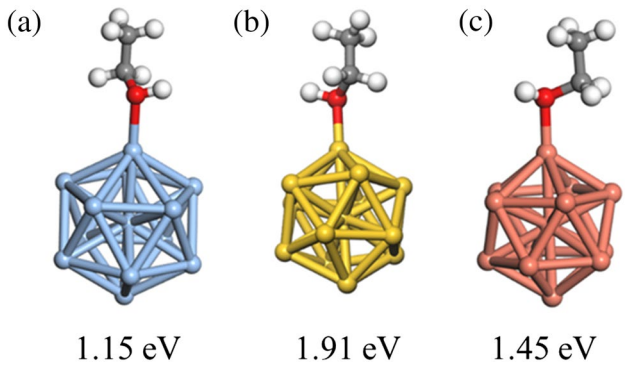

Fig. 2 Optimized structures of; **a** Ag_{13}–CH_3CH_2OH, **b** Au_{13}–CH_3CH_2OH, **c** Cu_{13}–CH_3CH_2OH, alongside their respective binding energies

complexes are 504.82, 307.41 and 2215.21 kcal/mol obtained for $LP^*(6)Ag_{11} \rightarrow LP^*(8)Ag_4$, $LP(7)Au_2 \rightarrow LP^*(6)Au_1$ and $LP^*(7)Cu_5 \rightarrow LP^*(9)Cu_2$ donor–acceptor interacting NBOs, respectively. Furthermore, the specific energies of stabilization for the bond formation between the metal atom in the clusters and O-atom in ethanol were 14.60, 26.21, and 79.67 kcal/mol for the $LP^*(8)Ag_4 \rightarrow \sigma^*Ag_5 - O_{14}$, $LP(6)Au_2 \rightarrow \sigma^*Au_5 - O_{14}$, and $LP(6)Cu_2 \rightarrow \sigma^*Cu_5 - O_{14}$ interacting NBOs, respectively.

QTAIM was employed to investigate the electron (ρ) and laplacian ($\nabla^2\rho$) of the electron density of the metal–oxygen bond formation along the bond critical path (BCP) [41]. The electron density at the BCP within the $Ag_5 - O_{14}$, $Au_5 - O_{14}$, and the $Cu_5 - O_{14}$ were 0.102, 0.085, and 0.111, respectively while the laplacian of the electron density were 0.652, 0.443, and 0.862. Charge delocalization were also analysed. The NBO charge delocalization for the $Ag_5 - O_{14}$, $Au_5 - O_{14}$, and $Cu_5 - O_{14}$ were 0.138, 0.445, and 0.089 e for Ag, Au, and Cu atoms, respectively and -0.776, -0.808, and -0.754 e for O-atoms bonded to the Ag, Au, and Cu, respectively.

Previous reports show that the Guerbet reaction proceeds through an aldol-type intermediate, whereby the reactant alcohol(s) is first dehydrogenated [42]. Aldol-type coupling followed by dehydration and hydrogenation produces the Guerbet saturated alcohol product [42, 43]. Moreover, we analysed the reaction coordinates of the clusters with C_2H_6O as shown in Fig. 3. The adsorption of the two ethanol molecules is an exothermic process, with Au_{13} showing the highest adsorption energy (− 3.14 eV) compared to Cu_{13} (− 1.75 eV) and Ag_{13} (− 2.13 eV). It is also clear that the activation of the ethanol molecule is an exothermic process, with activation barriers for the transfer of H atom to the clusters below 0.1 eV. The '$Cu_{13} + (C_2H_6O)_2$' reaction pathway has a relatively lower transition state energy barrier (0.02 eV). Then, the carbon atom on C_2H_5O attaches on to the carbon of C_2H_6O leading to formation of C_4H_9OH, with the intermediate steps having energies of − 2.89 eV, − 3.22 and − 1.77 eV for Ag_{13}, Au_{13} and Cu_{13} pathways, respectively. It was observed that each step of this pathway is thermodynamically favourable. To understand the pathway better, the energetic span model was used to evaluate its energy profile [24, 25]. The span model uses energy representations of different states of the cycle to generate the turnover frequency (TOF) [24, 25]. The TOF of a catalytic cycle is dependent on the TOF-determining intermediate

Table 2 The computed results for the second-order perturbation energy analysis. The atom numbers are indicated by the inserts

S/No.	Donor	Acceptor	E^2/(kcal/mol)	$\mathcal{E}_j - \mathcal{E}_i$	(Fi,j)
(a) Ag_{13}-C_2H_5OH					
1	$LP(6)Ag_{11}$	$LP^*(8)Ag_4$	504.82	0.02	0.133
2	$LP^*(6)Ag_{13}$	$LP^*(8)Ag_5$	465.76	0.01	0.097
3	$LP(6)Ag_7$	$LP^*(8)Ag_9$	381.44	0.03	0.148
4	$LP^*(6)Ag_{12}$	$LP^*(7)Ag_4$	319.68	0.04	0.158
5	$LP(6)Ag_{11}$	$LP^*(8)Ag_{12}$	250.39	0.03	0.132
(b) Au_{13}-C_2H_5OH					
1	$LP(7)Au_2$	$LP^*(6)Au_1$	307.41	0.06	0.141
2	$LP(7)Au_2$	$LP^*(6)Au_4$	276.90	0.06	0.133
3	$LP(6)Au_2$	$LP(6)Au_7$	252.46	0.04	0.100
4	$LP^*(6)Au_5$	$LP^*(9)Au_2$	238.43	0.20	0.311
5	$LP^*(8)Au_2$	$LP(6)Au_8$	210.31	0.07	0.124
(c) Cu_{13}-C_2H_5OH					
1	$LP^*(6)Cu_8$	$LP^*(6)Cu_{12}$	2215.21	0.02	0.276
2	$LP^*(6)Cu_{11}$	$LP^*(6)Cu_3$	1859.32	0.01	0.214
3	$LP^*(6)Cu_7$	$LP^*(6)Cu_1$	1494.82	0.01	0.203
4	$LP(6)Cu_9$	$LP^*(6)Cu_4$	1221.90	0.03	0.222
5	$LP^*(6)Cu_{12}$	$LP^*(6)Cu_3$	1556.28	0.01	0.184

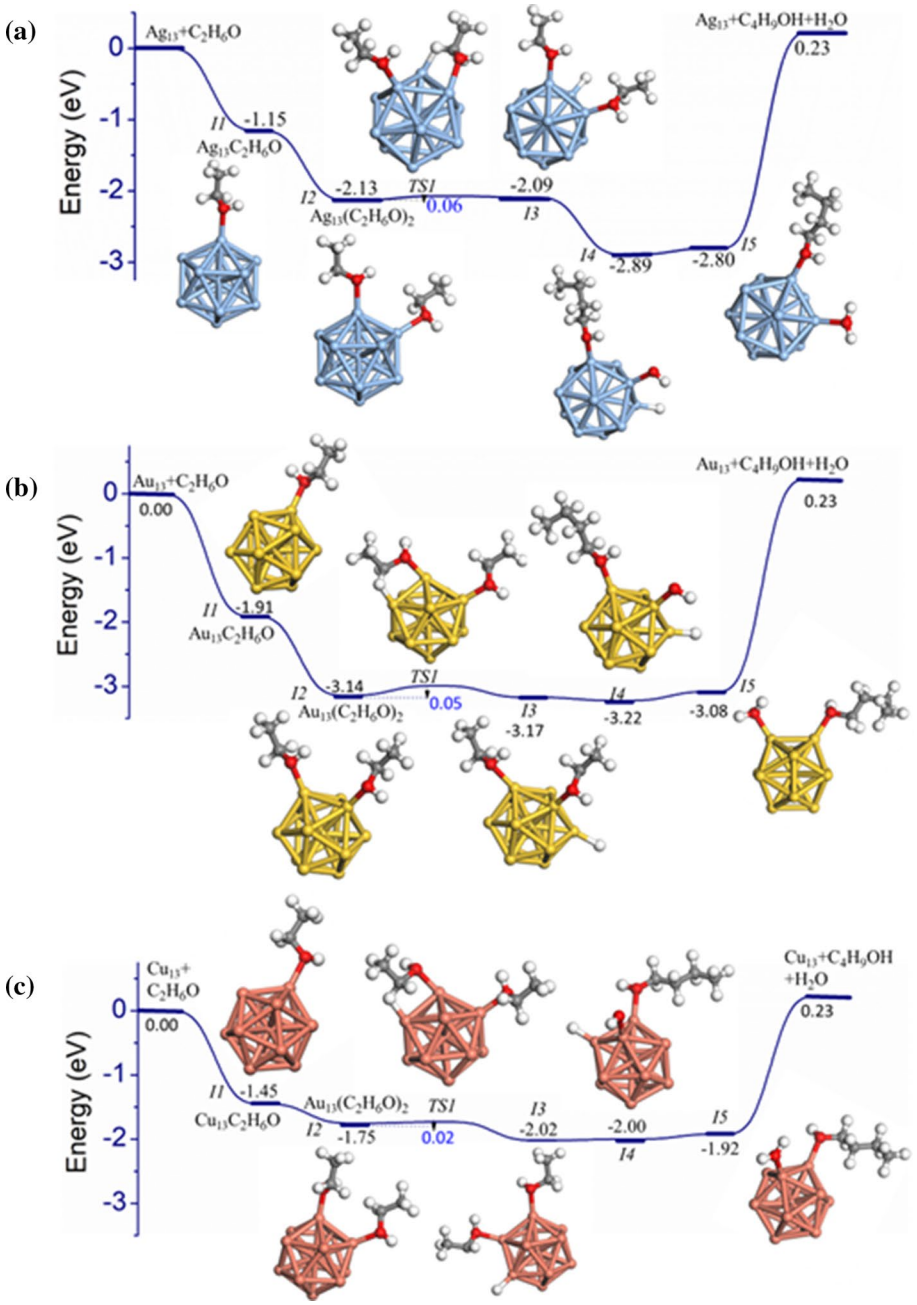

Fig. 3 The reaction coordinates of '$Au_{13}+(C_2H_6O)_2$', '$Ag_{13}+(C_2H_6O)_2$' and '$Cu_{13}+(C_2H_6O)_2$' in the coupling of C_2H_6O to C_4H_9OH

(TDI), and the TOF-determining transition state (TDTS) of the cycle [44]. The initial transition state, represented by the transfer of H atom from ethanol to the Ti cluster (*TS1*), is the maximum free-energy of the entire catalytic cycle [45]. Because TDI comes after *TS1*, then the energy span can is given by equation.

$$\delta E = T_{(TDTS)} - I_{(TDI)} + \Delta G_{rx},$$

where ΔG_{rx} is change in the free energy. It is seen that the calculated TOFs for $Cu_{13,}$ Au_{13} and Ag_{13} pathways are 0.5, 0.36 and 1.04 respectively.

In comparison, we have also considered the triangular structures of Cu_3, Ag_3 and Au_3. The frontier orbitals and corresponding geometry of Ag_3, Au_3 and Cu_3 clusters are shown in Fig. 4. The LUMO are generally at edge sites while the HOMO are at the center. The reaction coordinates of

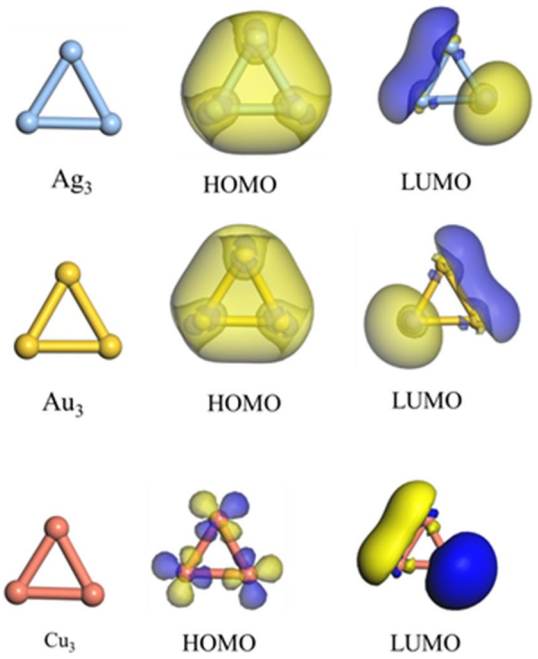

Fig. 4 Optimized structures and frontier orbitals of Ag_3, Au_3 and Cu_3

the triangular three atom clusters with C_2H_6O are given in Fig. 5. According to the energy profile, the adsorption of the two ethanol molecules is also exothermic, with Au_3 having the highest adsorption energy (− 1.93 eV) compared to Cu_3 (− 1.90 eV) and Ag_3 (− 1.25 eV). It is also clear that the activation of the ethanol molecule is an exothermic process, with transition state energy barriers for the transfer of H atom to the metal clusters ranging between 1.01 and 1.11 eV, which are relatively higher compared with those of the 13 atom clusters (0.02–0.06 eV. Then, the C atom on the carbonyl group attaches on to the carbon of C_2H_6O leading to formation of C_4H_9OH, with the intermediate steps having energies of − 1.20, − 1.11 and − 2.99 eV for Ag_3, Au_3 and Cu_3 pathways, respectively. Then H on the cluster binds to the –OH group, leading to the formation of H_2O. It is also seen that every elementary step of this pathway is thermodynamically favourable. These results agree with published literature reports on how gas phase metal clusters are excellent models for investigating the reaction mechanisms [10].

Having examined the binding and reaction of ethanol on typical coinage clusters, it is highly desirable to experimentally verify these findings. Fortunately, we synthesized and

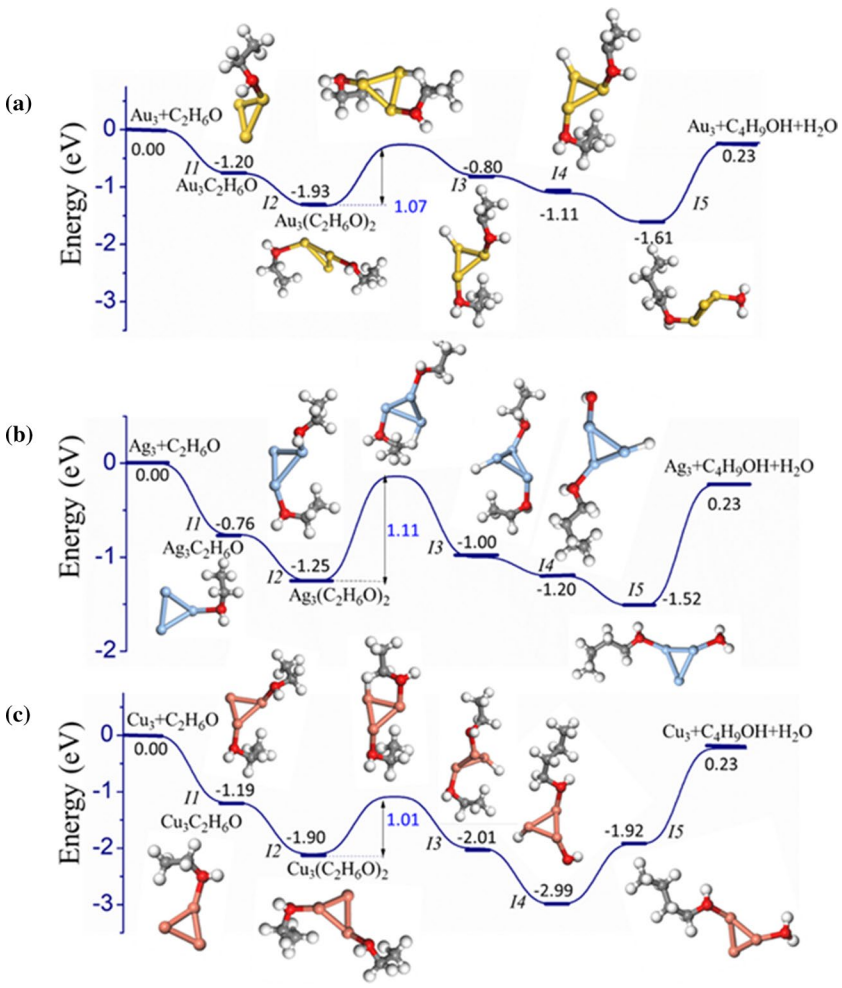

Fig. 5 The reaction coordinates of '$Ag_3 + (C_2H_6O)_2$', '$Au_3 + (C_2H_6O)_2$' and '$Cu_3 + (C_2H_6O)_2$' in the coupling of C_2H_6O to C_4H_9OH

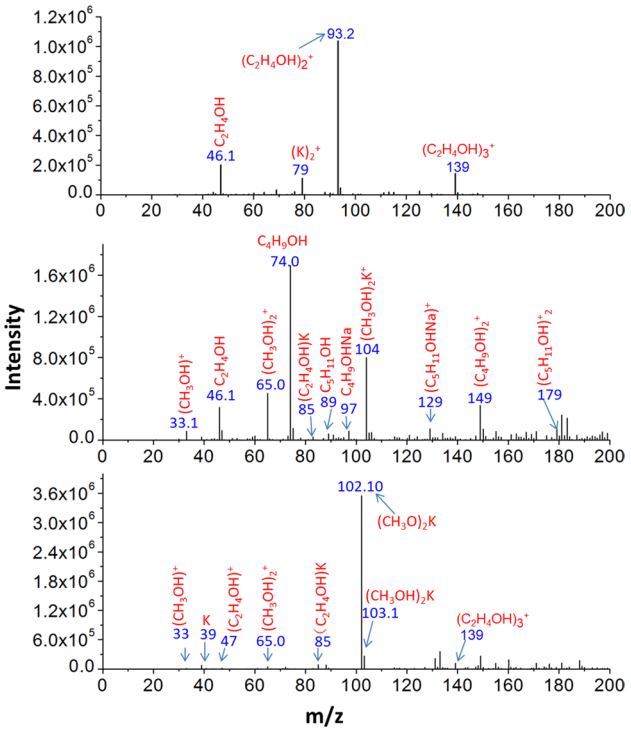

Fig. 6 ESI–MS spectra of: (*upper*) pure ethanol, (*middle*) ethanol after reaction with the Au clusters for 4 h at 70 °C (c) reaction of ethanol at 70 °C for 4 h in the absence of Au clusters, as an exclusion experiment

characterized chemically pure gold clusters by laser ablation in water [26, 27]. Figure 6, shows the mass spectra of ethanol, and the products after reacting with the chemically pure gold clusters. From the results, ethanol was converted to butanol. No coupling was observed in the blank experiment (Fig. 6c). Figure S1 also shows the mass spectra of ethanol before and after reacting with the gold clusters at various reaction times, whereby the products vary with the reaction duration. Figure 7 summarizes the catalytic performance of the Au clusters for ethanol conversion under different reaction times. The highest selectivity for butanol (61%) was obtained after a reaction time of 2 h while the highest ethanol conversion (91%) was obtained after a reaction time of 5 h. Similar findings have been reported fort gold and silver clusters as efficient models for catalytic reactions [46–51].

Conclusion

This study investigated the Guerbert reaction of ethanol to butanol on typical coinage clusters (i.e., copper, silver and gold). Using DFT calculations, we have examined the structure chemistry, bonding and reaction paths of the thirteen atom clusters and also the three atom clusters. Interestingly, Au allows for a slightly larger binding energy with ethanol. Furthermore, we have studied the ethanol coupling reactions using high resolution mass spectroscopy over the small Au cluster catalysts, prepared by laser ablation method followed by careful separation techniques. The observed coupling products agrees with the kinetic- and thermodynamic-allowed reaction pathways of Guerbet coupling of ethanol. The highest selectivity for butanol (61%) is obtained after a reaction time of 2 h while the highest ethanol conversion (91%) is obtained after a reaction time of 5 h.

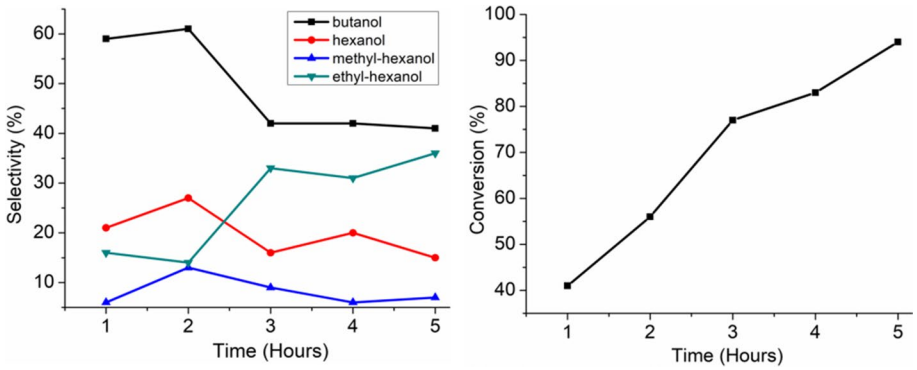

Fig. 7 Catalytic performance of the Au clusters for ethanol conversion under different reaction times; (*left*) product selectivity, (*right*) ethanol conversion

Supplementary Information The online version contains supplementary material available at https://doi.org/10.1007/s10876-022-02344-0.

Acknowledgements This work was also financially supported by Key Research Program of Frontier Sciences (CAS, Grant QYZDB-SSW-SLH024) and the National Natural Science Foundation of China (Grant No. 21722308).

Availability of Data and Material Supplementary data to this article can be found online.

Declarations

Conflict of interest The authors declare no conflict of interest.

References

1. M. Höök and X. Tang (2013). Depletion of Fossil Fuels and Anthropogenic Climate Change—a Review. *Energy Policy* **52**, 797–809.
2. T. T. Eaton (2013). Science-Based Decision-Making on Complex Issues: Marcellus Shale Gas Hydrofracking and New York City Water Supply. *Science of the Total Environment* **461**, 158–169.
3. B. G. Harvey and H. A. Meylemans (2011). The Role of Butanol in the Development of Sustainable Fuel Technologies. *Journal of Chemical Technology & Biotechnology* **86**, 2–9.
4. Szulczyk, K. R., Which Is a Better Transportation Fuel--Butanol or Ethanol? *International Journal of Energy & Environment* **2010**.
5. E. M. Green (2011). Fermentative Production of Butanol—the Industrial Perspective. *Current opinion in biotechnology* **22**, 337–343.
6. Guerbet, M., Condensation De L'alcool Isopropylique Avec Son Dérivé Sodé; Formation Du Méthylisobutylcarbinol Et Du Diméthyl-2.4-Heptanol-6. *Comptes rendus* **1909**, *149*, 129–132.
7. Y. Obora (2014). Recent Advances in A-Alkylation Reactions Using Alcohols with Hydrogen Borrowing Methodologies. *ACS Catalysis* **4**, 3972–3981.
8. Sun, Z.; Couto Vasconcelos, A. s.; Bottari, G.; Stuart, M. C.; Bonura, G.; Cannilla, C.; Frusteri, F.; Barta, K., Efficient Catalytic Conversion of Ethanol to 1-Butanol Via the Guerbet Reaction over Copper-and Nickel-Doped Porous. *ACS Sustainable Chemistry & Engineering* **2017**, *5*, 1738–1746.
9. K. M. Kosuda, A. Wittstock, C. M. Friend, and M. Bäumer (2012). Oxygen-Mediated Coupling of Alcohols over Nanoporous Gold Catalysts at Ambient Pressures. *Angewandte Chemie International Edition* **51**, 1698–1701.
10. Yin, B.; Luo, Z., Coinage Metal Clusters: From Superatom Chemistry to Genetic Materials. *Coordination Chemistry Reviews* **2020**, 213643.
11. Schenk, C.; Schnepf, A., Ge 14 [Ge (Sime 3) 3] 5 Li 3 (Thf) 6: The Largest Metalloid Cluster Compound of Germanium: On the Way to Fullerene-Like Compounds? *Chemical Communications* **2008**, 4643–4645.
12. C. L. Haynes and R. P. Van Duyne (2001). Nanosphere Lithography: A Versatile Nanofabrication Tool for Studies of Size-Dependent Nanoparticle Optics. *The Journal of Physical Chemistry B* **105**, 5599–5611.
13. G. López Arvizu and P. Calaminici (2007). Assessment of Density Functional Theory Optimized Basis Sets for Gradient Corrected Functionals to Transition Metal Systems: The Case of Small Ni N (N⩽ 5) Clusters. *The Journal of chemical physics* **126**, 194102.
14. P. Calaminici (2008). Is the Trend of the Polarizability Per Atom for All Small 3 D Transition Metal Clusters the Same? The Case of Ni N (N⩽ 5) Clusters. *The Journal of chemical physics* **128**, 164317.
15. Z. Xie, Q.-M. Ma, Y. Liu, and Y.-C. Li (2005). First-Principles Study of the Stability and Jahn-Teller Distortion of Nickel Clusters. *Physics Letters A* **342**, 459–467.
16. P. Rodríguez-Kessler and A. Rodríguez-Domínguez (2015). Stability of Ni Clusters and the Adsorption of CH_4: First-Principles Calculations. *The Journal of Physical Chemistry C* **119**, 12378–12384.
17. Dou, J.-H.; Sun, L.; Ge, Y.; Li, W.; Hendon, C. H.; Li, J.; Gul, S.; Yano, J.; Stach, E. A.; Dincă, M., Signature of Metallic Behavior in the Metal–Organic Frameworks M3 (Hexaiminobenzene) 2 (M= Ni, Cu). *Journal of the American Chemical Society* **2017**, *139*, 13608–13611.
18. B. Delley (1990). An All-Electron Numerical Method for Solving the Local Density Functional for Polyatomic Molecules. *The Journal of chemical physics* **92**, 508–517.
19. B. Delley (2000). From Molecules to Solids with the Dmol 3 Approach. *The Journal of chemical physics* **113**, 7756–7764.
20. P. Liu and J. A. Rodriguez (2005). Catalysts for Hydrogen Evolution from the [Nife] Hydrogenase to the Ni2p (001) Surface: The Importance of Ensemble Effect. *Journal of the American Chemical Society* **127**, 14871–14878.
21. N. Govind, M. Petersen, G. Fitzgerald, D. King-Smith, and J. Andzelm (2003). A Generalized Synchronous Transit Method for Transition State Location. *Computational materials science* **28**, 250–258.
22. Glendening, E.; Reed, A.; Carpenter, J.; Weinhold, F., Nbo Version 3.1, Tci. *University of Wisconsin, Madison* **1998**, *65*.
23. T. Lu and F. Chen (2012). Multiwfn: A Multifunctional Wavefunction Analyzer. *Journal of computational chemistry* **33**, 580–592.
24. A. Uhe, S. Kozuch, and S. Shaik (2011). Automatic Analysis of Computed Catalytic Cycles. *Journal of computational chemistry* **32**, 978–985.
25. S. Kozuch and S. Shaik (2006). A Combined Kinetic− Quantum Mechanical Model for Assessment of Catalytic Cycles: Application to Cross-Coupling and Heck Reactions. *Journal of the American Chemical Society* **128**, 3355–3365.
26. A. M. Pembere and Z. Luo (2017). Jones Oxidation of Glycerol Catalysed by Small Gold Clusters. *Physical Chemistry Chemical Physics* **19**, 6620–6625.
27. A. M. Pembere, M. Yang, and Z. Luo (2017). Small Gold Clusters Catalyzing the Conversion of Glycerol to Epichlorohydrin. *Physical Chemistry Chemical Physics* **19**, 25840–25845.
28. Y. Jia and Z. Luo (2019). Thirteen-Atom Metal Clusters for Genetic Materials. *Coordination Chemistry Reviews* **400**, 213053.
29. B. Jin, Y. Wang, C. Jin, J. J. De Yoreo, and R. Tang (2021). Revealing Au13 as Elementary Clusters During the Early Formation of Au Nanocrystals. *The Journal of Physical Chemistry Letters* **12**, 5938–5943.
30. M. B. Abreu, C. Powell, A. C. Reber, and S. N. Khanna (2012). Ligand-Induced Active Sites: Reactivity of Iodine-Protected Aluminum Superatoms with Methanol. *J. Am. Chem. Soc.* **134**, 20507–20512.
31. A. C. Reber, S. N. Khanna, P. J. Roach, W. H. Woodward, and A. W. Castleman (2010). Reactivity of Aluminum Cluster Anions with Water: Origins of Reactivity and Mechanisms for H_2 Release. *J. Phys. Chem. A* **114**, 6071–6081.
32. P. J. Roach, W. H. Woodward, A. W. Castleman, and Jr., Reber, A. C., Khanna, S. N., (2009). Complementary Active Sites Cause Size-Selective Reactivity of Aluminum Cluster Anions with Water. *Science* **323**, 492–495.

33. J. J. Melko, A. W. Castleman, and Jr., (2013). Photoelectron Imaging of Small Aluminum Clusters: Quantifying *S-P* Hybridization. *Phys. Chem. Chem. Phys.* **15**, 3173–3178.
34. X. Li, H. B. Wu, X. B. Wang, and L. S. Wang (1998). *S-P* Hybridization and Electron Shell Structures in Aluminum Clusters: A Photoelectron Spectroscopy Study. *Phys. Rev. Lett.* **81**, 1909–1912.
35. L. R. Domingo, P. Pérez, and J. A. Sáez (2013). Understanding the Local Reactivity in Polar Organic Reactions through Electrophilic and Nucleophilic Parr Functions. *RSC Advances* **3**, 1486–1494.
36. L. R. Domingo and P. Pérez (2014). A Quantum Chemical Topological Analysis of the C-C Bond Formation in Organic Reactions Involving Cationic Species. *Physical Chemistry Chemical Physics* **16**, 14108–14115.
37. L. R. Domingo and J. A. Sáez (2009). Understanding the Mechanism of Polar Diels-Alder Reactions. *Organic & biomolecular chemistry* **7**, 3576–3583.
38. J. A. Agwupuye, H. Louis, O. C. Enudi, T. O. Unimuke, and M. M. Edim (2022). Theoretical Insight into Electronic and Molecular Properties of Halogenated (F, Cl, Br) and Hetero-Atom (N, O, S) Doped Cyclooctane. *Mater. Chem. Phys.* **275**, 125239.
39. E. A. Bisong, H. Louis, T. O. Unimuke, J. O. Odey, E. I. Ubana, M. M. Edim, F. T. Tizhe, J. A. Agwupuye, and P. M. Utsu (2020). Vibrational, Electronic, Spectroscopic Properties, and Nbo Analysis of P-Xylene, 3, 6-Difluoro-P-Xylene, 3, 6-Dichloro-P-Xylene and 3, 6-Dibromo-Pxylene: Dft Study. *Heliyon* **6**, e05783.
40. E. D. Glendening, C. R. Landis, and F. Weinhold (2012). Natural Bond Orbital Methods. *Wiley interdisciplinary reviews: computational molecular science* **2**, 1–42.
41. Becke, A., *The Quantum Theory of Atoms in Molecules: From Solid State to DNA and Drug Design*; John Wiley & Sons, 2007.
42. J. T. Kozlowski and R. J. Davis (2013). Heterogeneous Catalysts for the Guerbet Coupling of Alcohols. *ACS Catalysis* **3**, 1588–1600.
43. M. J. Gines and E. Iglesia (1998). Bifunctional Condensation Reactions of Alcohols on Basic Oxides Modified by Copper and Potassium. *Journal of Catalysis* **176**, 155–172.
44. S. Kozuch and S. Shaik (2008). Kinetic-Quantum Chemical Model for Catalytic Cycles: The Haber− Bosch Process and the Effect of Reagent Concentration. *The Journal of Physical Chemistry A* **112**, 6032–6041.
45. L. Falivene, S. M. Kozlov, and L. Cavallo (2018). Constructing Bridges between Computational Tools in Heterogeneous and Homogeneous Catalysis. *ACS Catalysis* **8**, 5637–5656.
46. W. Fang, Q. Zhang, J. Chen, W. Deng, and Y. Wang (2010). Gold Nanoparticles on Hydrotalcites as Efficient Catalysts for Oxidant-Free Dehydrogenation of Alcohols. *Chemical Communications* **46**, 1547–1549.
47. T. Mitsudome, Y. Mikami, H. Funai, T. Mizugaki, K. Jitsukawa, and K. Kaneda (2008). Oxidant-Free Alcohol Dehydrogenation Using a Reusable Hydrotalcite-Supported Silver Nanoparticle Catalyst. *Angew. Chem. Int. Ed.* **120**, 144–147.
48. A. Nijamudheen, D. Jose, and A. Datta (2010). Why Does Gold (Iii) Porphyrin Act as a Selective Catalyst in the Cycloisomerization of Allenones? *The Journal of Physical Chemistry C* **115**, 2187–2195.
49. C.-R. Chang, Y.-G. Wang, and J. Li (2011). Theoretical Investigations of the Catalytic Role of Water in Propene Epoxidation on Gold Nanoclusters: A Hydroperoxyl-Mediated Pathway. *Nano Res.* **4**, 131–142.
50. S. M. Lang and T. M. Bernhardt (2011). Methane Activation and Partial Oxidation on Free Gold and Palladium Clusters: Mechanistic Insights into Cooperative and Highly Selective Cluster Catalysis. *Faraday discussions* **152**, 337–351.
51. S. M. Lang, T. M. Bernhardt, R. N. Barnett, and U. Landman (2010). Methane Activation and Catalytic Ethylene Formation on Free Au2+. *Angew. Chem. Int. Ed.* **49**, 980–983.